Optical Engineering

SPIEDigitalLibrary.org/oe

Ultrafast laser-induced damage and the influence of spectral effects

Jeremy R. Gulley

Ultrafast laser-induced damage and the influence of spectral effects

Jeremy R. Gulley
Kennesaw State University
Department of Biology and Physics
Box 1202
Kennesaw, Georgia 30144
E-mail: jgulley@kennesaw.edu

Abstract. Numerous studies have investigated the prerequisite role of photoionization in ultrafast laser-induced damage (LID) of bulk dielectrics. This study examines the role of spectral width and instantaneous laser frequency in LID using a frequency dependent multiphoton ionization (MPI) model and numerical simulation of initially 800 nm laser pulses propagating through fused silica. Assuming a band gap of 9 eV, MPI by an 800 nm field is a six-photon process, but when the instantaneous wavelength is greater than 827 nm an additional photon is required for photoionization, reducing the probability of the event by many orders of magnitude. Simulation results suggest that this frequency dependence can significantly impact the onset of LID and ultrashort pulse filamentation in solids. [DOI: 10.1117/1.OE.51.12.121805]

Subject terms: plasma generation; ultrashort pulse propagation; nonlinear optics; laser-induced damage; fused silica; nonlinear Schrödinger equation; computational optics; chirped laser pulse.

Paper 120405SSP received Mar. 15, 2012; revised manuscript received May 29, 2012; accepted for publication Jun. 7, 2012; published online Jun. 27, 2012.

1 Introduction

The past several decades have seen the advent of the commercial femtosecond laser system as well as the use of ultrashort laser pulses to affect precise changes in a variety of materials.[1,2] Ultrashort laser pulses are increasingly used for micro-machining,[3,4] the writing of waveguides and other structures in bulk dielectrics,[5–7] and also in medical procedures.[8,9] One critical aspect common to all of these applications is the initiation of laser-induced damage (LID) processes that lead to permanent changes in the material structure. It is generally assumed that the initiation of LID begins with the prerequisite process of photoionization, after which an optically significant plasma density is generated that gives rise to free-carrier absorption and impact ionization. Correct and practical modeling of impact ionization (or avalanching) during LID on the femtosecond time scale is still an open question in the literature.[10–18] However, the necessity of photoionization as a prerequisite to permanent LID stands in good agreement with nearly all models. Therefore, it is reasonable to assume that errors of many orders of magnitude in calculations of the photoionization rate threaten the validity numerical LID predictions. One such source of error is the spectral variance found in ultrashort laser pulses.

Photoionization calculations typically assume that a laser pulse is approximately monochromatic; that is $\Delta\omega/\omega_0 \ll 1$, where $\Delta\omega$ is the pulse's spectral width and ω_0 is a measure of the central frequency of the spectrum. However, one physical requirement of making a transform-limited pulsewidth shorter is that the corresponding spectral width will grow proportionately larger. If the pulsewidth approaches a single optical cycle of the laser field, as with ultrashort pulses, then the monochromatic approximation becomes questionable. The spectra of ultrashort pulses can also be significantly distorted by nonlinear optical effects during propagation. Processes such as self-phase modulation and ionization can broaden the spectrum and shift the central frequency away from its original value, see Fig. 1. The influence of these nonlinear processes on the pulse spectra, and the resulting spectral effects in ultrafast LID, are investigated in detail. The question addressed in this article is whether spectral widths, shifts, and temporal-pulse chirps can alter the initiation of bulk LID in a measurable way.

The results presented suggest that the spectral effects will alter both the location and shape of pre-critical electron-plasma formation in bulk fused silica. Spectral variance in the presented work either evolves by nonlinear propagation or is provided by initial-temporal chirps and pulse-widths. To model the dynamic evolution of these effects, simulations of ultrashort pulse propagation are performed in fused silica where the instantaneous frequency of the laser pulse is used in calculations of the photoionization rate. These results are compared to identical simulations of the kind ubiquitously performed in the literature. In these latter simulations the electron plasma evolution is calculated using the standard approximation that the pulse is monochromatic throughout the propagation.

2 Theory

The most common models of photoionization used in ultrafast LID calculations (the Keldysh[19] and PPT[20,21] models) include frequency dependence of the applied laser radiation. However, all of these models assume that the laser field is, at least approximately, monochromatic. When applicable, this condition ensures that the same number of photons must be absorbed for photoionization to occur in the multiphoton ionization (MPI) limit, regardless of the location in the material or the spatio-temporal position within the laser pulse. If a pulse's spectrogram remains narrowly symmetric about a central frequency then the MPI yield may not change significantly. In this case, the effect of absorbing low energy

0091-3286/2012/$25.00 © 2012 SPIE

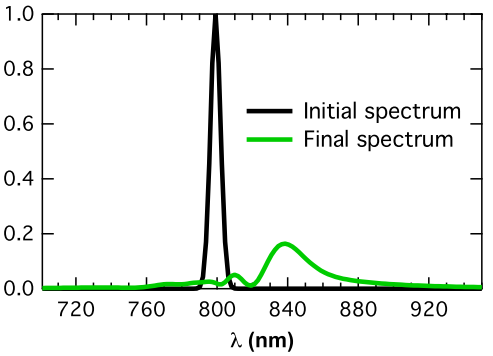

Fig. 1 Normalized initial and final on-axis spectra of a 140 fs, 800 nm laser pulse after 2.5 mm of propagation in fused silica. The pulse and material parameters used to generate these results are discussed in Sec. 3.

photons during MPI events would tend to offset the effect of also absorbing high energy photons.

However, for sufficiently broad spectra there exists the possibility of simultaneously absorbing only photons with energies much higher than those at the central frequency. This could decrease the number of such photons required for photoionization, thereby increasing the ionization rate accordingly. The opposite complication can occur for positively-chirped laser pulses where the leading pulse edge is red-shifted from the central frequency. In this case, an increase in the number of photons needed for MPI may occur and cause the photoionization rate to decrease by several orders of magnitude.

At moderately high intensities between the MPI and tunneling limits, the issue is further complicated in the Keldysh model[19] by the need to absorb a total energy greater than the effective band gap

$$U_{\text{eff}} = U + \frac{e^2|\xi|^2}{4m_e\omega^2}, \tag{1}$$

where U is the material band gap energy, the second term is the ponderomotive "wiggle" energy of the free carrier with charge e and effective mass m_e, $|\xi|$ is the laser field amplitude, and ω is the central optical frequency. In the multiphoton picture, the number of photons required for a photoionization event will be

$$n = \left\langle \frac{U_{\text{eff}}}{\hbar\omega} + 1 \right\rangle, \tag{2}$$

where the notation $\langle\cdot\rangle$ denotes the integer part. This condition ensures that the total number of photons required for photoionization will increase at high intensities in the MPI picture. This further implies that if the pulse frequency changes, then the MPI rate would change due to frequency dependence in the ponderomotive energy of Eq. (1) and the photon energy in Eq. (2). The following subsections will demonstrate that such alterations may lead to changes of many orders of magnitude in the MPI rate.

2.1 *Keldysh Model of Photoionization*

For the remainder of this work, the Keldysh photoionization rate for solids is used because in numerous studies it has provided good agreement with experiments of ultrashort laser pulse propagation in fused silica,[6,11,18,22–28] and fused silica will be the material referenced in this work. The photoionization formula developed by Keldysh for solids is[19]

$$W_{\text{PI}}(|\xi|,\omega;U,m) = \frac{2\omega}{9\pi}\left(\frac{m\omega}{\sqrt{\gamma_1}\hbar}\right)^{3/2} Q(\gamma,x) \times \exp[-\varpi\langle x+1\rangle]. \tag{3}$$

Here, the Keldysh parameter $\gamma = \omega\sqrt{mU}/e|\xi|$, $\gamma_1 = \gamma^2/(1+\gamma^2)$, $\gamma_2 = 1-\gamma_1$, $\varpi = \pi(K(\gamma_1) - E(\gamma_2))/E(\gamma_2)$, and $x = (2U/\pi\omega)(\sqrt{1-\gamma^2}/\gamma)E(\gamma_2)$. The functions $K(x)$ and $E(x)$ are complete elliptical integrals of the first and second kind, respectively, as defined in Ref. 29. The function $Q(\gamma,x)$ is given by

$$Q(\gamma,x) = \sqrt{\frac{\pi}{2K(\gamma_2)}}\sum_{n=0}^{\infty} \exp[-n\varpi]\Phi[\sqrt{\vartheta(n+2\nu)}],$$

where $\vartheta = \pi^2/4K(\gamma_2)E(\gamma_2)$, $\nu = \langle x+1\rangle - x$, and $\Phi(z) = \int_0^z \exp(y^2 - z^2)dy$ is the Dawson function.

The solid line in Fig. 2 shows the Keldysh photoionization rate as a function of the optical intensity in fused silica with a band gap of 9 eV and an effective mass equal to the rest electron mass. The dashed line in Fig. 2 shows the Keldysh six-photon ($n = 6$) MPI rate; $W_{\text{PI}} = \sigma_6 I^6$, where $\sigma_6 = 6.04\times10^{-47}$ $(\text{cm}^2/\text{W})^6\,\text{s}^{-1}\,\text{cm}^{-3}$ for the absorption of six 800 nm photons. Note that the Keldysh parameter γ is used to distinguish between the domains of MPI, $\gamma \gg 1$, and tunneling ionization, $\gamma \ll 1$. It is instructive to mention that at the intensity just below 4×10^{12} $\text{W}\,\text{cm}^{-2}$ in Fig. 2, MPI changes abruptly from a six-photon process to a 7-photon process, hence the order of magnitude change from the dashed six-photon MPI line. In the tunneling limit of high intensities for a particular frequency the photoionization rate approaches that of a static field.

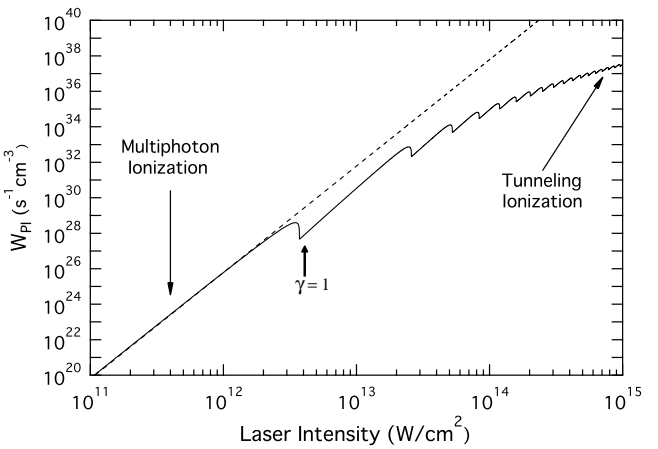

Fig. 2 The Keldysh photoionization rate as a function of laser intensity for 800 nm light in fused silica with a band gap of 9 eV. The solid line shows the full Keldysh expression, while the dashed line shows the common MPI rate that is valid at low intensities.

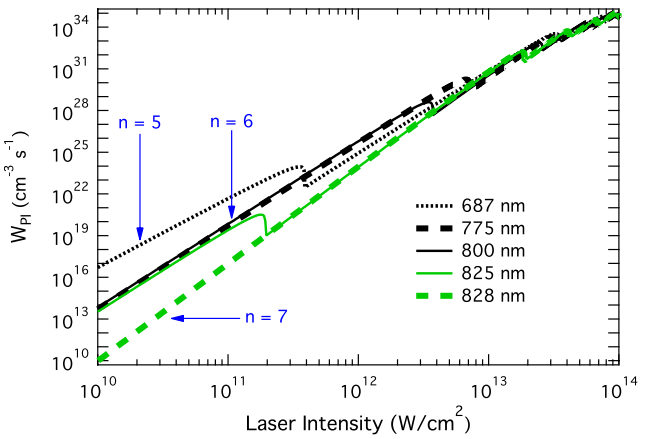

Fig. 3 Photoionization rates as a function of laser intensity for various wavelengths around 800 nm in fused silica with a band gap of 9 eV. For this material the $n = 5$, $n = 6$, and $n = 7$ regions [as defined by Eq. (2)] are represented in the MPI (low intensity) regime.

2.2 *Photoionization Rates for Neighboring Wavelengths*

To examine how different frequency components of an ultrashort laser pulse may affect the probability of photoionization, Fig. 3 shows the Keldysh photoionization rates for a field with a wavelength of 800 nm, as well as those for many neighboring wavelengths. Note that the 775, 800, and 825 nm wavelength rates are in good agreement for intensities in the MPI limit. This indicates that photoionization for the 140 fs laser pulse shown in Fig. 1, ranging spectrally from 790 to 810 nm, would be well approximated by simply using the rate for 800 nm in that limit. The same could be said for pulses as short as 50 fs that would still fit safely in the 775 to 825 nm spectral range. However, note the difference of 2 to 4 orders of magnitude between the 825 and 828 nm rates in the MPI limit. This is due to the fact that seven 828 nm photons are required to cross the band gap in the MPI limit, whereas only six 825 nm photons are required. Note also that after crossing an intensity of 2×10^{11} W/cm^2 the 825 nm rate falls from a six-photon rate to the 7-photon 828 nm rate. This is because an additional photon is required to cross the effective band gap at that intensity, as per Eq. (2). If large portions of a pulse's spectrum were to lie on two different sides of such a transitional wavelength or intensity then it is unlikely the photoionization rate could be well approximated by the rate for a single wavelength. Nevertheless, ultrafast photoionization rates in the literature are almost exclusively calculated for a single wavelength.

Ultrashort laser pulses propagating through fused silica often experience bulk damage thresholds on the order of 10^{13} W/cm^2.[6,18,23] Figures 2 and 3 show that those intensities lie in the intermediate regime of the Keldysh photoionization rate where both MPI and tunneling ionization play significant roles, with the role of the former declining at high intensity and the role of the latter increasing. At these intermediate intensities Fig. 3 shows that all of the photoionization rates begin to converge to a single frequency-independent tunneling rate. If avalanching also plays a significant role in ultrafast LID then order-of-magnitude changes resulting from spectral variance in the photoionization rate should occur at the leading edge of the pulse. There the intensity is lower and the precritical electron plasma is forming. Hence it is the initiation of LID which should first be examined to find the influence of spectral variance.

2.3 *Photoionization from Multi-Chromatic Fields*

The Keldysh model of photoionization was derived for a monochromatic laser field. To the author's knowledge there is no multi-chromatic model for nonlinear ionization in solids. This deficiency precludes the ability to accurately model MPI events involving many different frequencies. The standard practice in pulse propagation simulations is to calculate the Keldysh photoionization rate using a constant central frequency, but with a field amplitude that varies with time. In this article, the frequency used in the Keldysh rate is simply allowed with time as well, and is given by the instantaneous frequency. In this manner, a shift of the central pulse frequency can result in a changing photoionization rate.

There are three fundamental limitations in adopting such a model. First, all the material properties assumed in the Keldysh derivation are still assumed here, and are over simplified for most cases. Second, truly multi-chromatic MPI events are neglected since the frequency is assumed to have only one value at any particular time. This will give rise to artificially sharp changes in the MPI rate; for example, when an MPI transition wavelength is crossed. In a truly multi-chromatic model one could expect that the convoluted frequency combinations would lead to comparatively smoother transitions in the MPI limit. Third, although the instantaneous frequency is often a convenient quantity there are some situations in which it is not physically meaningful. See Ref. 30 for a summary on the nature and meaning of the instantaneous frequency.

3 Simulations

Simulations to model the effects of spectral width and temporal chirp on bulk LID are performed for ultrashort laser pulses propagating through 2.6 mm of fused silica. Variables and formulas referenced in this section are summarized in Table 1. Definitions and numerical values for the pulse and material parameters used in the simulations are summarized in Table 2. The simulations begin with a 20 μJ, 140 fs, 800 nm pulse that is loosely focused (100 μm beam waist) onto the front surface of a fused silica sample. During propagation in the sample the pulse undergoes catastrophic self-focusing and ends the simulated propagation having generated a plasma density approaching, but not exceeding, the critical density of 10^{21} cm^{-3} often associated with permanent damage. This simulated propagation is performed by solving for the complex envelope ξ of the linearly polarized, cylindrically symmetric electric field $\vec{E}$, defined by

$$\vec{E}(r,z,t) = \frac{1}{2}[\xi(r,z,t)e^{i(k_0 z-\omega_0 t)} + c.c.]\hat{x}.$$

The equation of propagation is derived in Ref. 31 and describes the evolution of ξ along the propagation axis z in the retarded time frame of the laser pulse, that is $\tau = t - z/v_g$, moving at the group velocity v_g.

Table 1 Definitions of variables.

Symbol	Definition
ξ	Electric field envelope
r	Beam radius coordinate
z	Propagation axis coordinate
τ	Retarded time coordinate
ω_0	Carrier frequency
$k(\omega)$	Wave vector
ρ	Free-carrier number density
σ	$e^2\tau_c/n_0 c\epsilon_0 m_r(1+\omega_0^2\tau_c^2)$
g	$-i\omega_0\tau_c/(1-i\omega_0\tau_c)$
U'	$(2-m_r/m_{e0})U_{\text{eff}}$
I	$I=(1/2)n_0\epsilon_0 c\lvert\xi\rvert^2$
k_m	$(\partial^m k/\partial\omega^m)_{\omega_0}$

$$\frac{\partial\xi}{\partial z}=\frac{i}{2k_0}\hat{T}^{-1}\nabla_\perp^2\xi+i\hat{D}_b\xi+i\frac{k_0\epsilon_0 c n_2}{2}\hat{T}\left[\int_{-\infty}^{\tau}d\tau' R(\tau-\tau')|\xi(\tau')|^2\right]\xi-\frac{\sigma}{2}(1+i\omega_0\tau_c)\hat{G}^{-1}[\rho\xi]-\frac{W_{\text{PI}}U}{2I}\xi. \quad (4)$$

Here $\hat{D}_b$ is a bound charge linear dispersion operator, $\hat{G}$ is a free-carrier dispersion operator, and $\hat{T}$ is a steepening operator defined, respectively, as

$$\hat{D}_b=\sum_{m=2}^{\infty}\frac{k_m}{m!}(i\partial_\tau)^m,$$

$$\hat{G}=1+i\frac{g}{\omega_0}\partial_\tau, \quad \text{and}$$

$$\hat{T}=1+i\frac{1}{\omega_0}\partial_\tau,$$

where linear absorption due to bound charges is neglected. The first term on the right hand side of Eq. (4) accounts for diffraction and linear shock, the second term accounts for dispersion due to bound charges, the third term represents contributions from the nonlinear polarization, the fourth term represents the contributions of free-carriers as calculated by the Drude model, and the fifth term accounts for absorption due to photoionization. The function $R(\tau)$ in the nonlinear polarization term is the delayed nonlinear optical response function from Ref. 32 and is given by

$$R(\tau)=(1-f_r)\delta(\tau)+f_r\frac{\tau_1^2+\tau_2^2}{\tau_1\tau_2^2}e^{-\tau/\tau_2}\sin(\tau/\tau_1),$$

Table 2 Values for parameters used in the simulations. Material parameters are those for fused silica.

Symbol	Description	Values	Units
λ	Initial wavelength	800	nm
τ_0	Initial pulsewidth	140	fs
β	Temporal chirp coefficient	0, $\pm 2\times10^{-3}$	rad/fs^2
w_r	Initial beam waist	100	μm
E_0	Initial pulse energy	20	μJ
n_0	Linear refractive index	1.45	
n_2	Nonlinear refractive index	2.48×10^{-16}	cm^{2}W^{-1}
f_r	Raman response fraction	0.18	
τ_1	Raman sinusoidal time	12.2	fs
τ_2	Raman decay time	32	fs
τ_r	Electron recombination time	150	fs
U	Material band gap	9	eV
m_{e0}	Electron rest mass	9.1×10^{-31}	kg
m_r	Reduced electron-hole mass	0.5	m_{e0}
m_e	Effective electron mass	1.0	m_{e0}
$\rho_{\max}$	Maximum electron density	6.6×10^{22}	cm^{-3}
τ_c	Free-carrier collision time	1.23	fs

where the first term represents an instantaneous electronic response, f_r is the fraction of the Raman contribution to the nonlinear polarization, and the constants τ_1 and τ_2 are adjustable parameters chosen to provide an adequate fit with the Raman-gain spectrum. The nonlinear polarization term in Eq. (4) accounts for self-focusing, self-phase modulation, self-steepening (nonlinear shock), and stimulated the Raman scattering.

Equation (4) is solved simultaneously with a rate equation describing the evolution of the free-carrier density ρ in the conduction band:[18]

$$\frac{d\rho}{dt}=\left(W_{\text{PI}}+\frac{\sigma I\rho}{U'}\right)\left(1-\frac{\rho}{\rho_{\max}}\right)-\frac{\rho}{\tau_r}. \quad (5)$$

This model includes contributions of photoionization, impact ionization (avalanching), and electron recombination. To produce a qualitative indication of the importance of spectral variation in the laser pulse, the Keldysh photoionization rate W_{PI} in Eqs. (4) and (5) are calculated by Eq. (3) using the instantaneous frequency of the laser pulse, that is $\omega(\tau)=\omega_0-\Im[(\partial_\tau\xi)/\xi]$, where the notation $\Im[\cdot]$ denotes the imaginary part. The plasma density generated by this simulation is then compared to that of an identical simulation

where the frequency is assumed to be $\omega(\tau) = \omega_0$, i.e., monochromatic when calculating Eq. (3). The simulations begin by constructing the electric field envelope at the beginning of the propagation, at which point the beam and pulse shapes are assumed to be Gaussian and are given by the formula

$$\xi(r,\tau,z=0) = \sqrt{\frac{2I_0}{\epsilon_0 c}}\exp\left[-\frac{r^2}{w_r^2} - \frac{2\ln(2)}{\tau_0^2}\tau^2 + i\frac{\beta}{2}\tau^2\right],$$

where $I_0 = E_0/(\pi/2)^{3/2}w_r^2\tau_0$ is the initial peak intensity. The initial temporal chirp of the pulse is determined by the parameter β which is positive for positively chirped pulses, negative for negatively chirped pulses, or zero for unchirped pulses.

4 Results

The intensity of the initially unchirped laser pulse at several locations during propagation is shown in Fig. 4. The figure captures the process of self-focusing as the pulse approaches $z = 2.5$ mm of propagation, at which point LID is being initiated. If the influence of beam asymmetries and material defects were to be included, it is likely that the pulse as seen in Fig. 4(d) would quickly undergo multiple filamentation.[33,34] Note also that the on-axis peak intensity in Fig. 4(d) of approximately 5×10^{13} W/cm^2 is at least an order of magnitude higher than that of the rest of the laser pulse off-axis. This implies that changes to the instantaneous frequency due to self-phase modulation will be an order of magnitude greater at the center of the beam than on the wings. Additionally, LID is most likely to occur where the intensity is highest; within a few micrometers of $r = 0$ in the beam structure for the results presented. However, integrating the intensity over this region gives only a small fraction of the pulse energy. This is demonstrated in the frequency domain by Fig. 5 which shows the normalized spectra of the pulses on-axis [Fig. 5(a) to 5(d)] as well as the complete pulse spectra [Fig. 5(e) to 5(h)] at various points during the propagation. To understand multi-chromatic LID effects in the simulations one must look at the on-axis spectra [Fig. 5(a) to 5(d)], as opposed to the complete spectra [Fig. 5(e) to 5(h)], of the laser pulses. In particular, note that the complete pulse spectra in Fig. 5 remain centered about the original central wavelength, which is not the case for the on-axis spectra.

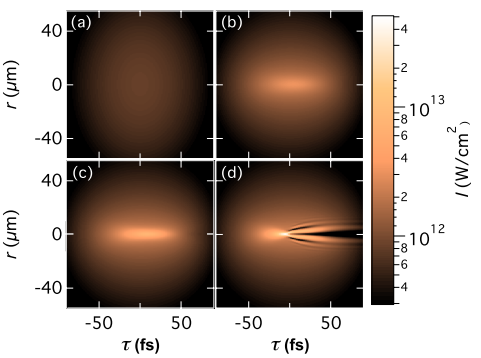

Fig. 4 Laser pulse intensity as a function of the beam radius r and temporal position τ for propagation distances of (a) $z = 0$ mm, (b) $z = 2.3$ mm, (c) $z = 2.4$ mm, and (d) $z = 2.5$ mm in fused silica.

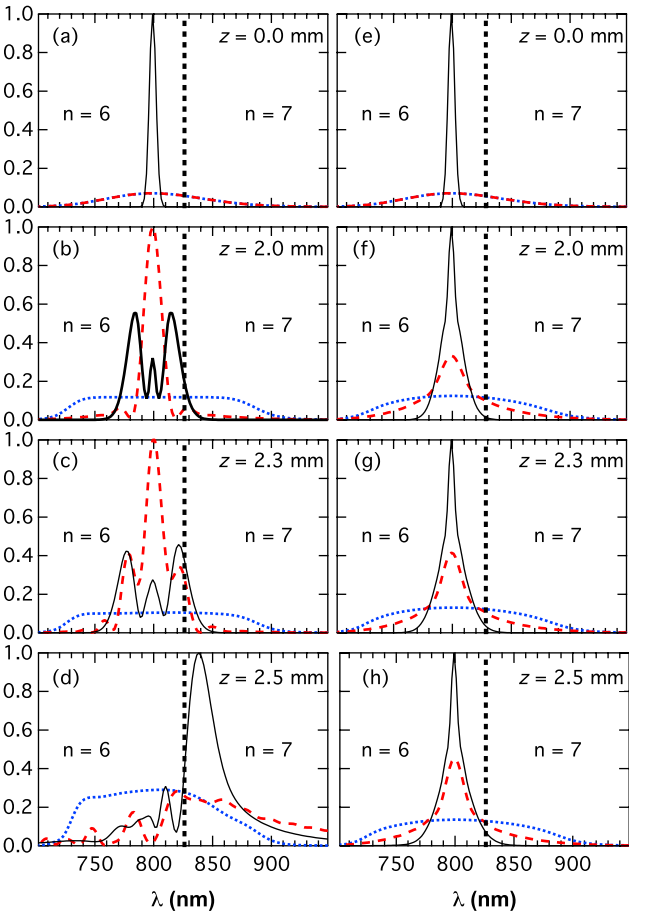

Fig. 5 (a) to (d) Normalized on-axis spectra and (e) to (h) complete on-axis spectra of the pulses. Initial pulse chirps are distinguished by the black-solid plots for unchirped, the red-dashed plots for negatively chirped, and the blue-dotted plots for positively chirped pulses. The dashed-black vertical line indicates the transition wavelength between the $n = 6$ and $n = 7$ MPI regions.

In Fig. [5(a) and 5(e)] the initial on-axis spectra and complete spectra, respectively, are identical because no nonlinear effects have occurred at the beginning of the propagation. Note also that the positively and negatively chirped pulses have identical spectra initially, although those frequencies are distributed oppositely in the time-domain. At $z = 2.0$ mm Fig. 5 shows significant deviation between the complete and on-axis spectra due to increased self-phase modulation at the beam center. In particular, for positive values of the nonlinear refractive index n_2, self-phase modulation will positively chirp the laser pulse as it propagates. This effect causes the spectrum of the negatively chirped pulse to narrow, and the spectra of the other pulses to broaden. Furthermore, linear dispersion will cause the negatively chirped pulse to undergo temporal compression while causing the other pulses to broaden in time proportionally to their initial or evolved positive chirps. These linear dispersion effects shift the respective nonlinear foci of the differently chirped pulses by hundreds of micrometers. This is shown in Figs. (6 to 8) which show the peak plasma densities generated at different positions along the propagation axis z.

In Fig. 5(d), most of the energy of the unchirped and negatively chirped pulses lie in the $n = 7$ MPI region. This spectral shift results from the "red-shifted" field on

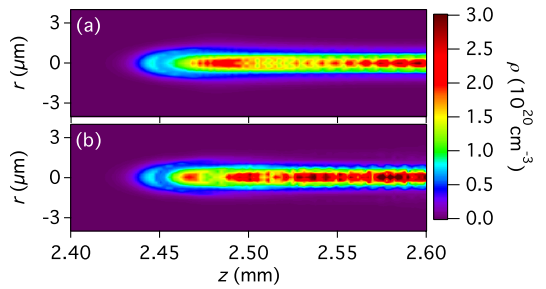

Fig. 6 Maximum plasma densities generated by the unchirped pulse after 2.4 mm of propagation in fused silica. A constant wavelength of 800 nm used in Eq. (3) for (a), while (b) uses the instantaneous frequency in Eq. (3).

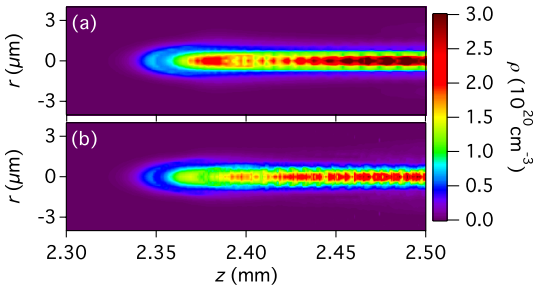

Fig. 8 Maximum plasma densities generated by the negatively chirped pulse after 2.3 mm of propagation in fused silica. A constant wavelength of 800 nm used in Eq. (3) for (a), while (b) uses the instantaneous frequency in Eq. (3).

the front edge of the laser pulse (a consequence of the nonlinear polarization), where the initial plasma density is being generated. The blue-shifted field on the trailing edge is largely absorbed and scattered by free-carriers as shown in Fig. 4(d). It is therefore highly questionable whether a photoionization rate for an 800 nm field is a valid approximation on the leading edge of the pulse at this point in the propagation. This red-shifting effect reduces the photoionization rate on the front edge of the pulse by 2 to 4 orders of magnitude, as demonstrated by Fig. 3. The results of such reductions in the photoionization rate are shown in Figs. 6 to 8, each of which compares calculations of peak generated plasmas using either a constant frequency or the instantaneous frequency in the photoionization model.

Figures 6 to 8 show the maximum plasma density generated in the material near the end of propagation for each of the initial pulse chirps. In each of these figures part (a) represents calculations using only an 800 nm wavelength in the Keldysh model, while part (b) uses the instantaneous frequency. Note that in Fig. 6(b) there is a range of about 20 μm between $z = 2.47$ mm and $z = 2.49$ mm where the plasma density is less than half the value of Fig. 6(a). This same feature occurs also in Figs. 7 and 8, and is a direct result of self-phase modulation "red-shifting" the front pulse edge into the $n = 7$ MPI region thereby causing plasma generation to decline. Further into the material, Figs. 7 and 8 also show that spectral ionization effects visibly alter the balance between self-focusing and plasma defocusing that characterize pulse filamentation in the medium. Although the peak plasma densities do not exceed the frequently assumed value for permanent damage of 10^{21} cm^{-3}, they are approaching this value within an order of magnitude. This

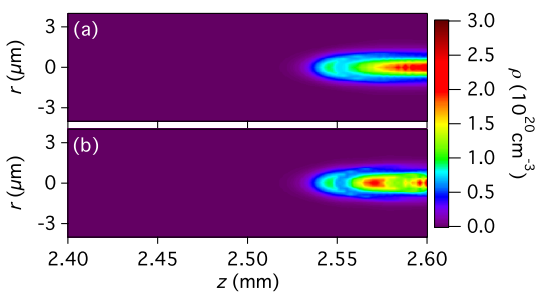

Fig. 7 Maximum plasma densities generated by the positively chirped pulse after 2.4 mm of propagation in fused silica. A constant wavelength of 800 nm used in Eq. (3) for (a), while (b) uses the instantaneous frequency in Eq. (3).

range of plasma generation has previously been associated with both irreversible and annealable modifications to the local refractive index.[23] When viewed in the context of femtosecond-laser micromachining or nanofabrication in the bulk, the aforementioned 20 μm range of discrepant predictions for the generated plasma is not a trivial matter. The difference of hundreds of micrometers resulting from different initial chirps from otherwise identical pulses also warrants careful consideration. A post mortem examination of this material region will be able to distinguish the resulting permanent changes to the local refractive index.

5 Discussion

The results suggest that spectral effects on LID initiation are demonstratively significant. However, this issue has received comparatively little attention in the literature. There are at least two reasons why this might be the case. The first is best demonstrated by a comparison of the complete spectra and the on-axis spectra of Fig. 5. Note that from $z = 2.0$ mm to $z = 2.5$ mm, the complete spectra change very little, despite the statio-temporal dynamics involved in self-focusing and filamentation. Although the complete spectra broaden during the propagation, most of the pulse energy remains in the $n = 6$ MPI spectral region. This shows that one should not rely only on the spectrum of the complete pulse as a measure of chromatic integrity. Otherwise, one can significantly misrepresent the field-material interaction in the region where LID or filamentation will occur. This is especially true if the pulse is strongly chirped. Therefore, when calculating the plasma evolution great care should be taken to account for the local spectrum in the region of concern.

The second reason this issue has received comparatively little attention may be that, to the author's knowledge, there is no model of photoionization or avalanching that was derived to account for pulses of arbitrary shape, temporal width, and phase. The Keldysh model was derived for a monochromatic CW field;[19] as was the kinetic (Fokker-Planck) equation for the evolution of free-carriers in energy space[35,36] and the simplified rate equation that was derived from it[12] [Eq. (5) is a variation of this model]. Even a more recently proposed multi-rate equation model for avalanching, developed by Rethfeld[16,17] specifically with ultrashort laser pulses in mind, still depends on the assumption of an approximately monochromatic field. The presented results suggest that, without a multi-chromatic model of

laser-induced ionization, our current understanding of bulk LID by ultrashort pulses is fundamentally limited.

In this article, the author has used an *ad hoc* modification of the Keldysh photoionization rate for solids by performing calculations with the instantaneous frequency instead of a single unchanging frequency. The author emphasizes that this *ad hoc* modification should not be regarded as a permanent substitute for new comprehensive models of ultrafast ionization in solids. The Keldysh model of photoionization was not derived with the assumption of a changing frequency, therefore the results of Figs. 6 to 8 are an admittedly qualitative demonstration. Furthermore, the modified Keldysh approach of this work takes no account of multi-frequency absorption events that ultimately contribute to the total MPI yield. For such cases it has yet to be determined if a closed analytic formula, such as Eq. (3) or Eq. (5), can be derived for an ultrashort laser pulse of arbitrary shape and phase. Such formulas would be extremely useful for quantitative predictions of ultrafast LID and filamentation in solids.

6 Conclusion

The validity of using photoionization rates derived for monochromatic fields to calculate ultrafast LID has been investigated by inspection and simulation. In the MPI limit, there are transitional wavelengths about which the number of photons required for photoionization changes by a single integer value, reducing or increasing the probability of the event by orders of magnitude. If the spectrum of an ultrashort laser pulse straddles such a transitional wavelength, it is doubtful that a photoionization rate for a single frequency will accurately describe the initial generation of free-carriers. In the special case of fused silica with a band gap of 9 eV, the transitional wavelength from a six-photon process to a 7-photon process occurs at approximately 827 nm. Given this condition, it was shown that MPI rates would be well approximated by simply using the rate for an 800 nm field in the case of a transform-limited 800 nm laser pulse as short as 50 fs. However, 800 nm pulses shorter than 50 fs would straddle the 827 nm transition, as would longer but strongly chirped ultrashort pulses.

Simulations were performed to examine the influence of nonlinear self-frequency shift and initial pulse chirps on the initiation of LID in bulk dielectrics. Self-focusing and dispersion effects in fused silica produced on-axis spectra with much greater variance compared to the complete pulse spectra. Propagation simulations using the instantaneous frequency to calculate photoionization rates were compared to corresponding simulations using a constant 800 nm wavelength for that purpose. When pre-damage plasma absorption and defocusing became appreciable for an initially unchirped pulse, the resulting on-axis spectrum had shifted into a region requiring an addition photon for photoionization in the MPI limit. However, the energy on the wings of the pulse, and thus the total spectrum, remained centered about the initial frequency.

For the case of initially chirped pulses, both linear and nonlinear optical effects distort the originally identical spectra. The location and shape of resulting plasma distributions in the material were also altered by these effects. It was found that the initial chirps combined with linear dispersion effects to shift the location of potential damage sites by hundreds of micrometers. The on-axis spectral evolution, driven by nonlinear optical effects, generated different shapes for the maximum plasma densities in the material when comparing the monochromatic and instantaneous frequency photoionization models, and were critical to modeling the pulse filamentation dynamics. These results among others[37–39] demonstrate the urgent need for new models of LID that account for the multi-frequency nature of ultrashort laser pulses.

References

1. R. W. Boyd, *Nonlinear Optics*, 2nd ed., Academic Press, San Diego, CA (2002).
2. J.-C. Diels and W. Rudolf, *Ultrashort Laser Pulse Phenomenon: Fundamentals, Techniques, and Applications on a Femtosecond Time Scale*, 2nd ed., Academic Press, San Diego, CA (2006).
3. C. B. Schaffer et al., "Micromachining bulk glass by use of femtosecond laser pulses with nanojoule energy," *Opt. Lett.* **26**(2), 93–95 (2001).
4. C. B. Schaffer and E. Mazur, "Micromachining using ultrashort pulses from a laser oscillator," *Opt. Phot. News* **12**(4), 20–23 (2001).
5. Y. Shimotsuma et al., "Self-organized nanogratings in glass irradiated by ultrashort light pulses," *Phys. Rev. Lett.* **91**(24), 247405 (2003).
6. S. W. Winkler et al., "Transient response of dielectric materials exposed to ultrafast laser radiation," *Appl. Phys. A* **V84**(4), 413–422 (2006).
7. X. Zhu et al., "Influence of laser parameters and material properties on micro drilling with femtosecond laser pulses," *Appl. Phys. A* **V69**(7), S367–S371 (1999).
8. A. Vogel et al., "Mechanisms of femtosecond laser nanosurgery of cells and tissues," *Appl. Phys. B* **81**(8), 1015–1047 (2005).
9. D. Giguère et al., "Laser ablation threshold dependence on pulse duration for fused silica and corneal tissues: experiments and modeling," *J. Opt. Soc. Am. A* **24**(6), 1562–1568 (2007).
10. M. Lenzner et al., "Femtosecond optical breakdown in dielectrics," *Phys. Rev. Lett.* **80**(18), 4076–4079 (1998).
11. M. Mero et al., "Scaling laws of femtosecond laser pulse induced breakdown in oxide films," *Phys. Rev. B* **71**(11), 115109 (2005).
12. B. C. Stuart et al., "Nanosecond-to-femtosecond laser-induced breakdown in dielectrics," *Phys. Rev. B* **53**(4), 1749–1761 (1996).
13. A.-C. Tien et al., "Short-pulse laser damage in transparent materials as a function of pulse duration," *Phys. Rev. Lett.* **82**(19), 3883–3886 (1999).
14. T. Q. Jia et al., "The ultrafast excitation processes in femtosecond laser-induced damage in dielectric omnidirectional reflectors," *J. Appl. Phys.* **100**(2), 023103 (2006).
15. F. Quéré, S. Guizard, and P. Martin, "Time-resolved study of laser-induced breakdown in dielectrics," *Europhys. Lett.* **56**(1), 138–144 (2001).
16. B. Rethfeld, "Free-electron generation in laser-irradiated dielectrics," *Phys. Rev. B* **73**(3), 035101 (2006).
17. B. Rethfeld, "Unified model for the free-electron avalanche in laser-irradiated dielectrics," *Phys. Rev. Lett.* **92**(18), 187401 (2004).
18. A. Q. Wu, I. H. Chowdhury, and X. Xu, "Femtosecond laser absorption in fused silica: numerical and experimental investigation," *Phys. Rev. B* **72**(8), 085128 (2005).
19. L. V. Keldysh, "Ionization in the field of a strong electromagnetic wave," *Sov. Phys. JETP* **20**(5), 1307–1314 (1965).
20. A. M. Perelomov, V. S. Popov, and M. V. Terent'ev, "Ionization of atoms in an alternating electric field: II," *Sov. Phys. JETP* **24**(1), 207–217 (1967).
21. A. M. Perelomov, V. S. Popov, and M. V. Terent'ev, "Ionization of atoms in an alternating electric field: I," *Sov. Phys. JETP* **23**(5), 924–934 (1966).
22. L. Berge, S. Skupin, and G. Steinmeyer, "Temporal self-restoration of compressed optical filaments," *Phys. Rev. Lett.* **101**(21), 213901 (2008).
23. A. Couairon et al., "Filamentation and damage in fused silica induced by tightly focused femtosecond laser pulses," *Phys. Rev. B* **71**(12), 125435 (2005).
24. L. Sudrie et al., "Femtosecond laser-induced damage and filamentary propagation in fused silica," *Phys. Rev. Lett.* **89**(18), 186601 (2002).
25. B. H. Christensen and P. Balling, "Modeling ultrashort-pulse laser ablation of dielectric materials," *Phys. Rev. B* **79**(15), 155424 (2009).
26. A. Kaiser et al., "Microscopic processes in dielectrics under irradiation by subpicosecond laser pulses," *Phys. Rev. B* **61**(17), 11437–11450 (2000).
27. J. Liu, R. Li, and Z. Xu, "Few-cycle spatiotemporal soliton wave excited by filamentation of a femtosecond laser pulse in materials with anomalous dispersion," *Phys. Rev. A* **74**(4), 043801 (2006).
28. P. Polesana et al., "Near-field dynamics of ultrashort pulsed bessel beams in media with kerr nonlinearity," *Phys. Rev. E* **73**(5), 056612 (2006).
29. M. Abramowitz and I. A. Stegun, *Handbook of Mathematical Functions*, 10th ed., Dover, New York (1964).

30. B. Boashash, "Estimating and interpreting the instantaneous frequency of a signal. I. fundamentals," *Proc. IEEE* **80**(4), 520–538 (1992).
31. J. R. Gulley and W. M. Dennis, "Ultrashort-pulse propagation through free-carrier plasmas," *Phys. Rev. A* **81**(3), 033818 (2010).
32. K. J. Blow and D. Wood, "Theoretical description of transient stimulated Raman scattering in optical fibers," *J. Quant. Electr.* **25**(12), 2665–2673 (1989).
33. V. Kandidov et al., Chapter 15 in *Self-Focusing: Past and Present*, Vol. **114** of Topics in Applied Physics, pp. 371–398, Springer, New York, NY (2009).
34. J. R. Gulley et al., "Interaction of ultrashort-laser pulses with induced undercritical plasmas in fused silica," *Phys. Rev. A* **85**(1), 013808 (2012).
35. L. H. Holway, "High-frequency breakdown in ionic crystals," *J. Appl. Phys.* **45**(2), 677–683 (1974).
36. L. H. Holway, "Temporal behavior of electron distributions in an electric field," *Phys. Rev. Lett.* **28**(5), 280–283 (1972).
37. V. Gruzdev, "Ultrafast laser-induced modifications of energy bands of non-metal crystals," *Proc. SPIE* **7504**, 75040G (2009).
38. M. Turowski et al., "Laser-induced damage and nonlinear absorption of ultrashort laser pulses in the bulk of fused silica," *Proc. SPIE* **7504**, 75040H (2009).
39. E. Louzon et al., "Reduction of damage threshold in dielectric materials induced by negatively chirped laser pulses," *Appl. Phys. Lett.* **87**(24), 241903 (2005).

Jeremy Gulley is an assistant professor of physics at Kennesaw State University near Atlanta, Georgia. His research is in theoretical applied physics and computational ultrafast optics. In particular, his research concentrates on simulating the propagation of high intensity ultrashort laser pulses through bulk nonlinear media. These simulations are used to investigate laser-induced dielectric breakdown, pulse filamentation, and ultrafast laser-induced modifications to bulk solids.